Large Eddy Simulation of Diluted Turbulent Spray Combustion Based on FGM Methodology: Effect of Fuel and Mass Loading

Amsini Sadiki, Mouldi Chrigui, Fernando Sacomano and Assaad R. Masri

Abstract A numerical methodology relying on Large Eddy Simulation is used to analyze and evaluate the impact of fuel and mass loading on turbulent spray combustion. To retrieve the flow, mixing and combustion proper-ties, an Eulerian-Lagrangian approach is adopted. The method includes a full two-way coupling between the interacting two phases in presence, while the evaporation process is described by a non-eqnilibrium vaporization model. The carrier phase turbulence is captured by a combustion LES technique in which first order sub-grid scale models are applied.

Two different fuels are used to produce spray jets through a pilot flame and a co-flowing atmospheric air. A spray pre-evaporation zone enables the combustion regime to turn from diffusion to partially premixed mode. The first liquid fuel is acetone, preferred for its ability to vaporize quickly. It is modeled by a detailed reaction mechanism including 84 species and 409 elementary reactions. The ethanol as second fuel is widely used as alternative fuel. It is modeled by a detailed reaction mechanism consisting of 56 species and 351 reversible reactions. To reduce the computational costs, the combustion is described by means of a detailed tabulated chemistry approach according to the Flamelet Generated Manifold (FGM) strategy. The occurring flow and combustion properties are numerically analyzed and compared with experimental data for both fuels under different mass loading conditions. The impact of fuel and mass loading on turbulent spray combustion is evaluated in terms of flame structure, exhaust gas temperature, droplet velocities and diameters, droplet velocity fluctuations, and spray volume flux at different distances from the exit planes.

A. Sadiki (✉) · M. Chrigui · F. Sacomano
Institute for Energy and Power plant Technology, Department of Mechanical Engineering,
TU Darmstadt, Jovanka-Bontschits-Str. 2, 64287 Darmstadt, Germany
e-mail: sadiki@ekt.tu-Darmstadt.de

M. Chrigui
Research Unit Materials, Energy and Renewable Energies,
University of Gafsa, Gafsa, Tunisia

A. R. Masri
School of Aerospace, Mechanical and Mechatronic Engineering,
The University of Sydney, Sydney, NSW 2006, Australia

B. Merci, E. Gutheil (eds.), *Experiments and Numerical Simulations of Turbulent Combustion of Diluted Sprays,* ERCOFTAC Series 19, DOI 10.1007/978-3-319-04678-5_5,

1 Introduction

Advanced low emission combustion chamber strategies are under development in order to meet the necessity for transportation and power generation industries to fulfill stringent regulations concerning pollutants emissions. These concepts are sensitive to variable time- and space uniformity of fuel vapor composition inherent to liquid fuels used. These time- and space varying fuel properties (in the vapor and in liquid phase) affect substantially the vaporization and kinetics-related processes, like ignition, flame propagation/stability and pollutants level. As such issues when designing combustion systems for liquid fuel are essential for the understanding of flame ignition and extinction and the prediction of pollutant formation and emission [1, 3, 14, 17, 19, 24, 27, 28, 30, 31, 40, 43, 45, 49, 52], an accurate modeling of these phenomena reqnires taking into account turbulence, heat transfer, fuel spray evaporation and detailed chemistry effects. In this contribution, numerical modeling based on Large Eddy Simulation (LES) is applied to investigate combustion processes of single component liquid spray jets.

Comprehensive reviews of LES combustion models in reacting single phase flows are provided in [18, 36, 37]. Extensive fundamental and applied researches were especially dedicated to address questions that govern the interacting phenomena in reactive multiphase flows. A recent review is provided by Sadiki et al. [40]. Pera et al. [32] and Zoby et al. [52] among others have proved a strong interdependence between combustion and disperse phase properties and highlighted the difficulty of isolating physical effects. Beside these studies, outstanding studies were also carried out in the modeling of spray ignition [45], [28], [49], reacting DNS [31, 45], [52], Conditional Moment Closure [24], [27], [26] DNS/LES coupling and transported filtered density function [14, 17, 19] of turbulent sprays. With respect to chemistry it appears that it is not realistic for engineering applications to solve transport eqnations for all species occurring in the chemical reaction process. Reduction techniques are often favored. Thereby one group is formed by the flamelet based tabulated chemistry along with the Flamelet Generated Manifold (FGM) (see e.g. [11, 47, 48, 50]) or the Flamelet Prolongated ILDM [13]. Though considerable efforts have been accomplished, applications of FGM based combustion modelling have not yet been done, to our knowledge, for spray combustion coupled to LES. Only recently Chrigui et al. [7] and Chrigui et al. [9] published their first achievements using LES to investigate spray jet flames of acetone and ethanol fuels. They focused on demonstrating the feasibility of classical LES coupled to an Eulerian-Lagrangian spray module to capture flow and combustion properties.

The present work aims at using this LES-based Eulerian-Lagrangian methodology to assess the impact of fuel and mass loading on the combustion properties of turbulent spray jets. Two different fuels, acetone and ethanol, are used to produce the spray jets through a pilot flame and a co-flowing atmospheric air. A spray pre-evaporation zone enables the combustion regime to turn from diffusion to partially premixed spray combustion. The methodology includes a full two-way coupling of the interacting two phases in presence, while the carrier phase turbulence is captured by the LES and the combustion by the FGM approach. The droplet evaporation is described by a non-eqnilibrium vaporization model along with a droplet Lagrangian tracking.

The paper is structured as follows. First the droplet Lagrangian tracking is introduced, followed by an outline of the non-eqnilibrium evaporation model. Then the modeling approach of LES completed by the FGM generation is highlighted. In section 3, the experimental configuration and the computational set up including the boundary conditions for both the carrier and the disperse phases are presented. Analysis, discussion and comparisons of the numerical results with the experimental data are provided in the subseqnent section while conclusions are summarized in the final section.

2 Modeling Approach

2.1 Disperse Phase Lagrangian Description

According to the Lagrangian approach, the eqnations of the droplet position x_{pi}, velocity u_{pi} and temperature T_p along the trajectory of each computational droplet in the carrier flow field have to be solved. Assuming a spherical, single parcel these eqnations are:

$$\frac{\mathrm{dx_{pi}}}{\mathrm{dt}} = \mathrm{u_{pi}}\,, \qquad \mathrm{m_p}\frac{\mathrm{du_{pi}}}{\mathrm{dt}} = \mathrm{F}_i \tag{1}$$

$$\mathrm{m_p C_p}\frac{\mathrm{dT_p}}{\mathrm{dt}} = \mathrm{Q} \quad \text{and} \quad \frac{\mathrm{dm_p}}{\mathrm{dt}} = -\dot{\mathrm{m}}_{\mathrm{vap}} \tag{2}$$

where $m_p$is the mass of computational droplet or parcel, C_p the heat coefficient, F_i denotes the summation of all the forces acting on the parcel and Q the net rate heat transfer to the parcel while $\dot{m}_{vap}$ expresses the droplet vaporization rate, respectively. Since the ratio between the specific mass of liquid fuel and that of the gas phase mixture has a value around 10^3, we follow Chrigui et al. [7] and consider only the drag, gravitation and buoyancy forces to act on the droplet. Eq. (1) that describes the particle dynamics according to the Basset-Boussinesq-Oseen eqnation (BBO-eqnation) then reduces to:

$$\frac{du_{p,i}}{dt} = \frac{3}{4}\frac{C_W}{D_p}\frac{\rho}{\rho_p}\left|\overrightarrow{u} - \overrightarrow{u_p}\right|(u_i - u_{p,i}) + \frac{(\rho_p - \rho)}{\rho_p}g_i \tag{3}$$

The drag coefficient $C_W$is determined for a spherical, not deformable, droplet as proposed by Yuen and Chen (1976):

$$C_W = \frac{24}{\mathrm{Re}_p}\left(1 + \frac{1}{6}\mathrm{Re}_p^{2/3}\right) \qquad \mathrm{Re}_p \le 1000 \tag{4}$$

$$C_W = 0.44\mathrm{Re}_p \geq 1000$$

where Re_p denotes the particle Reynolds number given by

$$\mathrm{Re}_p = \frac{D_p \left|u_i - u_{pi}\right|}{\nu}. \quad (5)$$

while the first term in (3) includes the particle-relaxation time, τ_d, expressed as

$$\tau_d = \frac{4D_d \rho_d}{3C_W \, \bar{\rho} \, |u_i - u_{pi}|} \quad (6)$$

Thereby D_d is the particle diameter, ρ_d the density of particle and ν the kinematic viscosity of the fluid.

It is worth mentioning that in Eq. (3) the flow velocity u_i appears in its instantaneous value.To quantify this instantaneous fluid velocity and its effect on the droplet distribution within the LES framework, the SGS values of the fluid parcel velocity at the droplet location should be modeled. As it is known from recent studies by Pozorski et al. [38] the impact of SGS dispersion can vary depending on the particle inertia parameter. In particular, for evaporating spray flow, the droplets become smaller and their inertia parameter changes, hence sooner or later the droplets unavoidably enter the size range where there is an impact from the flow SGS. In LES, reports from the literature highlighted the importance of the SGS in the prediction of the disperse phase properties (see in [7, 9, 19]). Though the SGS dispersion appears to be so relevant for the prediction of the reacting two phase flow, it is common practice in the Eulerian-Lagrangian LES studies of dispersed flows to neglect the SGS flow scales [2, 3, 19, 30, 43]. It is generally argued that the long-time particle dispersion is governed by the resolved, larger-scale fluid eddies. In this contribution the dispersion of droplet is not accounted for. We simply rely on the fact that at least 80 % of the instantaneous carrier phase turbulence level is captured by the resolved scales.

While writing Eq. (2) temperature variation inside the droplet is neglected and thus droplet temperature is considered uniform. This assumption is reasonable since dragged droplets have diameters in the range of 30 μm. Accordingly the Uniform Temperature (UT) model by Abramzon et al. [1] and Sirignano [46] is applied to describe the droplet evaporation process. This model describes the evolution of droplet's temperature and diameter, i.e. evaporation rate and energy flux through the liquid/gas interface. The non-eqnilibrium extension of this model is applied (see [25, 41]). Note that all the assumptions of this model are valid in the investigated configurations. In particular, break-up and coalescence are neglected to ensure that the evolution of the droplet diameter is only due to the evaporation processes. The Weber number (We) near the nozzle (x/D = 0.3), which is used as an indicator for the break-up phenomenon, is less than 0.3 in the configurations under study. The critical value, however, is about 40 times larger, i.e. $\mathrm{We}_{\mathrm{cri}} = 12.07$. The Ohnesorge Number (Oh) is less than 0.006 for all cases at the exit plane, therefore no further drop deformation and break up are possible downstream of the exit plane and thus the changes in the droplet size are due to evaporation only. Reviews of the evaporation models can be found in [1], [46], [4], [44] and [25].

2.2 LES Description

In the line of the FGM approach, the filtered transport eqnations for control variables, namely the mixture fraction and one reaction progress variable (RPV), are solved together with the filtered transport eqnations for mass density and momentum of the Newtonian fluid under investigation in a variable-density Low Mach number formulation as:

$$\frac{\partial \bar{\rho}}{\partial t} + \frac{\partial \bar{\rho}\tilde{u}_i}{\partial x_i} = \bar{S}_{vapor} \tag{7}$$

$$\begin{aligned} &\frac{\partial}{\partial t}(\bar{\rho}\tilde{u}_i) + \frac{\partial}{\partial x_j}(\bar{\rho}\tilde{u}_i\tilde{u}_j) = -\frac{\partial \bar{p}}{\partial x_i} + \bar{\rho}g_i + \\ &\frac{\partial}{\partial x_j}\left[\bar{\rho}\tilde{\nu}\left(\frac{\partial \tilde{u}_i}{\partial x_j} + \frac{\partial \tilde{u}_j}{\partial x_i}\right) - \frac{2}{3}\bar{\rho}\tilde{\nu}\frac{\partial \tilde{u}_k}{\partial x_k}\delta_{ij} - \bar{\rho}\tau_{ij}^{sgs}\right] + \bar{S}_{u,i} \end{aligned} \tag{8}$$

$$\frac{\partial}{\partial t}\bar{\rho}\tilde{z} + \frac{\partial}{\partial x_i}(\bar{\rho}\tilde{u}_i\tilde{z}) = \frac{\partial}{\partial x_i}\left(\bar{\rho}\tilde{D}_f\frac{\partial \tilde{z}}{\partial x_i}\right) - \frac{\partial}{\partial x_i}(\bar{\rho}J_i^{sgs}) + \bar{S}_{vapor} \tag{9}$$

$$\begin{aligned} &\frac{\partial}{\partial t}\bar{\rho}\tilde{Y}_{RPV} + \frac{\partial}{\partial x_i}\left(\bar{\rho}\tilde{u}_i\tilde{Y}_{RPV}\right) = \frac{\partial}{\partial x_i}\left(\bar{\rho}\tilde{D}\frac{\partial \tilde{Y}_{RPV}}{\partial x_i}\right) \\ &\qquad -\frac{\partial}{\partial x_i}\left(\bar{\rho}J_i^{sgs}\right) + \tilde{\dot{\omega}}_{RPV} + \tilde{\dot{\omega}}_{vapor} \end{aligned} \tag{10}$$

where the dependent filtered variables are obtained from spatial filtering, $\phi = \tilde{\phi} + \phi''$ with $\tilde{\phi} = \overline{\rho\phi}/\bar{\rho}$ and ϕ'' the subgrid scale (SGS) fluctuations. Thereby bars and tildes express mean and filtered quantities. In Eqs. (7)-(10) the variables u_i (i = 1, 2, 3) denote the velocity components at x_i direction, ρ the density, p the hydrostatic pressure and δ_{ij} the Kronecker delta. The quantity ν is the kinematic molecular viscosity and D_f the molecular diffusivity coefficient. Following Chrigui et al. [7] the mixture fraction, z, is defined according to Bilger et al. [5] as:

$$z = \frac{a - a_{Oxidizer}}{a_{Fuel} - a_{Oxidizer}} \tag{11}$$

where

$$a = 2\frac{Y_C}{M_{w,C}} + 0.5\frac{Y_H}{M_{w,H}} - \frac{Y_O}{M_{w,O}}. \tag{12}$$

The parameters Y_C, Y_H and Y_O denote the element mass fractions of carbon, hydrogen and oxygen atoms. $M_{w,C}$, $M_{w,H}$ and $M_{w,O}$ are the molecular weights. At the inlet the values of the oxidizer and fuel are given by $a_{Oxidizer}$ and a_{Fuel}, respectively.

Table 1 Source terms due to the presence of droplets

ψ	$\tilde{S}_{\psi,i}$
1	$\sum_p \frac{\dot{m}_{p,v} N_p}{V_{i,j,k}}$
$\tilde{u}$	$-\sum_p \frac{\dot{m}_p N_p}{V_{i,j,k}} [\left(u_p^{t_n+\Delta t}\right) - u_p^{t_n}) - g_x\ \Delta t] + \sum_p \frac{\dot{m}_{p,v} N_p}{V_{i,j,k}}\ u_p^{t_n}$
$\tilde{v}$	$-\sum_p \frac{\dot{m}_p N_p}{V_{i,j,k}} [\left(v_p^{t_n+\Delta t}\right) - v_p^{t_n}) - g_y\ \Delta t] + \sum_p \frac{\dot{m}_{p,v} N_p}{V_{i,j,k}}\ v_p^{t_n}$
$\tilde{w}$	$-\sum_p \frac{\dot{m}_p N_p}{V_{i,j,k}} [\left(w_p^{t_n+\Delta t}\right) - w_p^{t_n}) - g_z\ \Delta t] + \sum_p \frac{\dot{m}_{p,v} N_p}{V_{i,j,k}}\ w_p^{t_n}$
$\tilde{z}$	$\sum_p \frac{\dot{m}_{p,v} N_p}{V_{i,j,k}}$

The quantity $\tilde{Y}_{RPV}$ is the filtered concentration of the reaction progress variable and D denotes the molecular diffusivity coefficient. The Eqs. (7)-(10) govern the evolution of the large, energy-carrying, scales of flow and scalar field. The effect of the small scales in the flow and scalar field appears through the SGS stress tensor and the SGS scalar flux vector

$$\tau_{ij}^{SGS} = u_i u_j - u_i u_j \tag{13}$$

$$J_i^{sgs} = u_i \xi - u_i \xi,\ \xi \equiv (z, Y_{RPV}) \tag{14}$$

respectively. The SGS stress tensor is postulated by a Smagorinsky-model with dynamic procedure according to Germano et al. [15]. In order to stabilize the model, the modification proposed by Sagaut [42] is applied. In addition a clipping approach will reset negative Germano coefficient C_s to zero to avoid destabilizing values of the model coefficient. It is known that wall-adaptive SGS models have been proposed recently, like wall adapting laminar eddy (WALE) model or the Vreman model with and without dynamic procedure, see [42]. Nevertheless, no special wall-treatment is included in the SGS model. We rather rely on the ability of the dynamic procedure to capture the correct asymptotic behavior of the turbulent flow when approaching the wall [51]. To represent the SGS scalar flux in the mixture fraction and in the RPV eqnations a gradient ansatz (15) is used with a constant turbulent Schmidt number of 0.7.

$$J_i^{sgs} = -\frac{\upsilon_t}{\sigma_t}\frac{\partial \tilde{\xi}}{\partial x_i}; \upsilon_t = C_s \Delta^2 \left|\overline{S}\right| \tag{15}$$

υ_t is SGS viscosity, σ_t SGS Schmidt number and $\left|\overline{S}\right|$ the absolute values of strain rate.

The source terms $\overline{S}_{u,i}$ and $\overline{S}_{vapor}$ that characterize the direct interaction of mass, momentum, and mixture fraction between the droplets and the carrier gas are summarized in Table 1. The variable ψ represents the mass density, velocity components (u, v, w) and the mixture fraction, respectively. The quantities, $\tilde{u}$, $\tilde{v}$ and $\tilde{w}$, are the filtered gas phase (axial, tangential and transversal) velocity components while u_p, v_p and w_p represent the corresponding velocity components of the parcel. N_p is the number of real droplets represented by one numerical droplet and V_{ijk} the cell volume. The quantity g represents the gravitation, $\dot{m}_p$ the amount of mass released by a parcel when it crosses a control volume (CV) per second while Δt stands for the Lagrangian integration time step.

Concentrating on Eq. (10), notice that the term, $\tilde{\dot{\omega}}_{RPV}$, represents the classical filtered chemical reaction rate [13, 18, 35, 36, 37, 33, 48] and the last term accounts for the evaporation contributions into the RPV eqnation [32]. Some other additional terms may emerge in a general expression of the RPV eqnation that explicitly includes the effect of evaporation on combustion [32]. Assuming that all droplets have evaporated before combustion, only the quantity $\tilde{\dot{\omega}}_{RPV}$ needs further modeling within the FGM approach. In the present work the RPV is defined as

$$Y_{RPV} = \frac{Y_{CO_2}}{M_{CO_2}} + \frac{Y_{H_2O}}{M_{H_2O}} + \frac{Y_{H_2}}{M_{H_2}}, \tag{16}$$

where Y_{CO_2}, Y_{H_2O} and Y_{H_2} are the mass fraction of CO_2, H_2O and H_2, respectively. The quantity M represents the molar mass, so its reciprocal is used as a weighting factor for each species. As pointed out elsewhere, the choice of the species defining the RPV depends on the problem being solved. In this specific case, the three major species retained are considered to properly capture the reaction zone. Using the two parameters (z, Y_{RPV}) a two-dimensional manifold is then generated by means of the CHEM1D code [6] by simply simulating a set of 1D diffusion flamelets [6, 13, 20, 33, 35, 48, 50] with increasing scalar dissipation rate, and thereafter switching to unsteady flamelets when reaching the critical scalar dissipation rate.

The filtered combustion variables required in the LES are then retrieved by integrating over the joint PDF of the mixture fraction and the defined RPV:

$$\tilde{\phi} = \int_0^\infty \int_0^\infty \phi(z, y) P(z, y) dz\, dy; \quad \mathrm{y} \equiv \mathrm{Y}_{RPV}. \tag{17}$$

where, $P(z, y)$ is the joint PDF. It is practical to carry out the pre-integration upon the normalized values, where the RPV is normalized by its maximum value restricting the integration domain to lie in [0, 25]. Assuming a statistical independence between the RPV and the mixture fraction yields:

$$\tilde{\phi} = \int_0^1 \int_0^1 \phi(z, y) \tilde{P}(z) \tilde{P}(y^*) dz\, dy^* \tag{18}$$

where the Favre-weighted PDF is derived from a standard one, $\widetilde{P}\left(y^*\right) = \rho\left(y^*\right) P\left(y^*\right) \big/ \bar{\rho}$, and y^* the normalized RPV. Since the mixture fraction is no more a conservative quantity, it may influence the PDF distributions. Gutheil et al. [14, 17] showed from a comparison of Monte-Carlo PDF with standard *beta*-PDF that a *beta*-function describes the actual shape of the PDF differently. Nevertheless a presumed *beta*-PDF distribution is chosen here as crude approximation. This implies the mixture fraction depends on its first and second moments. Effects of this assumption on predicted RANS results were reported in [20]. In LES, these have not been investigated in the literature yet.

In Eq. (18) the PDF of the RPV needs to be estimated. As a first-order approach, the δ-function is applied, allowing the combustion variables to be function of the

RPV mean values only. This assumption implies that the fluctuations of the RPV are sufficiently resolved or they could be omitted. This is realistic for spray flames under study, since they tend to exhibit diffusion flame behavior in which the RPV fluctuations are not large compared to premixed cases. The joint PDF in (2, 17) yields

$$P(z, y^*) = P(z) \cdot P(y^*) = \beta(z; \tilde{z}, z''^2) \cdot \delta(y^*) = P(z; \tilde{z}, z'',^2 y^*). \tag{19}$$

Thermo-chemical quantities in Eq. (2, 17) can then be parameterized and tabulated in so-called pre-integrated tables (tabulated SGS chemical parameters) as function of filtered mixture fraction, its variance and normalized filtered RPV as:

$$\tilde{\phi} = f(\tilde{z}, z'',^2 y^*). \tag{20}$$

While generating the FGM table, the effect of droplet evaporation along with the interaction between evaporating droplets and combustion is not directly accounted for. To do this, at least the vaporized mass quantity has to be included as parameter in Eq. (20). This work is still in progress.

The reliability of spray combustion models depends primarily on how the fuel-air mixture preparation is accurately described. It is then of interest to better understand the behavior of vapor concentration along with the mixture fraction variance when spray evaporation is present. To this purpose, a transport eqnation of mixture fraction variance is suitable [31, 32, 39]. Sadiki et al. [39] investigated the impact of the modeling of the evaporation source term in the transport eqnation of mixture fraction variance on the prediction of combustion properties in RANS context. Thereby the outcomes of two models have been compared. It turned out that the model by Reveillon et al. [31] could deliver more accurate prediction in comparison to the formulation by Hollman et al. (see in [39]). Because the proper contribution of the evaporation source term in the eqnation of the RPV (see Eq. (10)) has been neglected as complete evaporation has been assumed before combustion, the mixture fraction variance is obtained simply following the algebraic gradient formulation [7, 35]

$$z''^2 \approx {C_{eq}}^2 \left(\frac{\partial \tilde{z}}{\partial x_i} \right)^2 \tag{21}$$

The model coefficient, C_{eq}, lies into [0.1, 0.2] and is set to 0.15 in the present work.

The combustion of acetone is modeled by a detailed reaction mechanism including 84 species and 409 elementary reactions as developed in [34]. Ethanol is modeled by means of a detailed chemical reaction mechanism as developed and validated by Marinov [22]. It consists of 56 species and 351 reactions.

3 Investigated Configurations and Numerical Set Up

3.1 Experimental Configuration and Computational Sset Up

The configuration used to study the ethanol and acetone spray combustion is shown in Fig. 1. It represents the setup experimentally investigated by Masri and Gounder

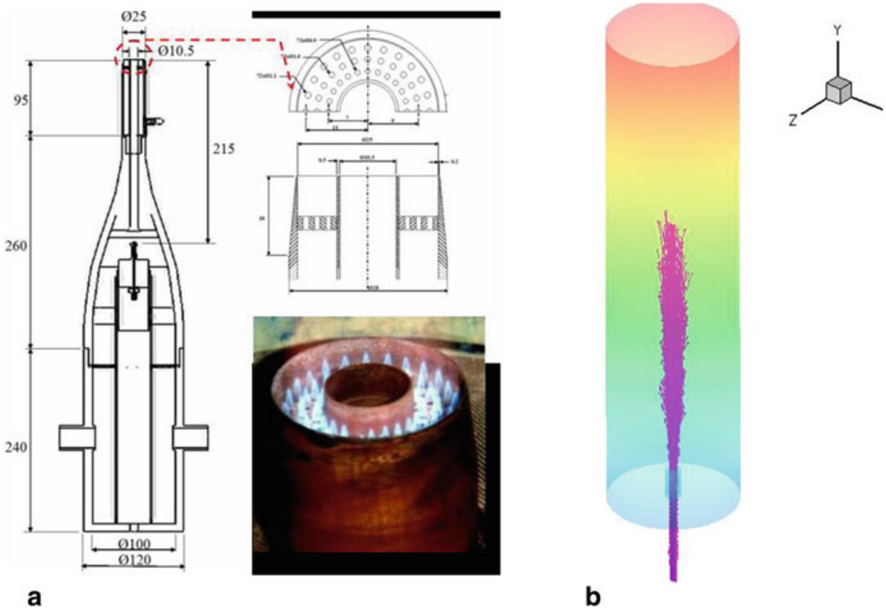

Fig. 1 **a** Schematic of the spray [40] burner set up **b** Computational domain

[16, 23]. The burner is mounted vertically in a wind tunnel that supplies a co-flowing air stream of 4.5 m/s. The co-flow of diameter 104 mm surrounds the burner. The contraction of the carrier phase topology has a ratio of 10:1. The outer diameter of the annulus is 25.0 mm whereas the lip thickness is 0.2 mm. The pilot flame that is set to a stoichiometric mixture of hydrogen, acetylene and air has an un-burnt bulk velocity of 1.5 m/s. Its border is mounted 7 mm upstream of the nozzle exit and contains 72 holes. The co-flow and nozzle exit plane is 59.0 mm downstream of the tunnel exit plane. This provides an unconfined working section.

The spray is initialized 215 mm upstream of the nozzle exit plane and exhibits a poly-disperse behavior after traveling a pre-vaporization zone in which small classes evaporate before reaching the exit of the nozzle. The resulting ethanol and acetone flames feature a partially premixed character. A detailed description of the experimental setup and apparatus used for the generation of the experimental data is provided by Masri and Gounder [23] (see also [16, 47]).

In [26] the non-reacting and reacting cases SP1, SP2 and EtF1, EtF4 and EtF7 have been investigated using RANS and CMC. Applying RANS and FGM, Chrigui et al. [8] studied the configurations SP1/AcF1, SP2/AcF2 and SP5/AcF5. Using LES, Chrigui et al. analyzed recently the evaporation process of the configurations EthF1, EthF3, EthF6 and EthF8 (see in this book) and the spray combustion of AcF3, AcF6 and AcF8 [7]. They kept the same liquid fuel injection rate while varying the jet Reynolds number as well as the carrier mass flow rate along with the spray jet density. They also reported LES results of the configurations EtF3 and EtF8 in [9, 40].

Table 2 Different test cases with the flow boundary conditions using both fuels, acetone and ethanol, respectively

Acetone Combustion	*Flame test case AcF3*	*Flame test case AcF6*
$\dot{m}_l[g/\min]$	45	45
$U_{jet}[m/s]$	24	36
$\dot{m}_{air}[g/\min]$	150	225
$\mathrm{Re}_{jet}[-]$	20730	28076
$\phi_{golbal}[-]$	2.9	1.9
Ethanol Combustion	*Flame test case EtF3*	*Flame test case EtF6*
$\dot{m}_l[g/\min]$	45	45
$U_{jet}[m/s]$	24	36
$\dot{m}_{air}[g/\min]$	150	225
$\mathrm{Re}_{jet}[-]$	19678	28076
$\phi_{golbal}[-]$	2.9	1.9

In the present chapter, a LES-based study is carried out in which the configurations EtF3 and EtF6 fueled with ethanol as well as AcF3 and AcF6 using acetone are compared in terms of fuel influence and mass loading impact on the combustion properties.

3.2 Boundary Conditions

All the boundary conditions for the carrier phase are provided in Table 2. A decreasing mass loading in the inner jet from 30 to 15 % could be calculated. The velocity components of the carrier phase are given as block profile at the inlets and the Reynolds numbers from Table 2 attest a highly turbulent two phase flow. As the carrier phase travels a distance 20D to reach the nozzle exit plane, the flow develops turbulent structures, even with block velocity profiles.

Following Chrigui et al. [7, 9, 40] the configuration under study was numerically represented by a computational domain consisting of 17 blocks that count 1.1×10^6 control volumes (cv), Fig. 1b. Within one coupling time step the number of parcels injected is 2500 while the number of time steps achieved between both phases, that represent the fluid data and/or source term transfer, exceeds 320,000 couplings. The averaging of the spray properties is thus performed over more than 750×10^6 parcels. The disperse phase properties are statistically independent and not conditioned on the number of parcels tracked or coupling time steps. The TVD scheme is applied for the velocity exit boundary with a condition with 6 m/s. For the RPV the boundary condition is set to zero in the entire domain except at the pilot flame inlet, where it is set to the maximum absolute value that eqnals 0.0101. Note that the total number of the tracked parcels exceeded 1 million within one coupling-iteration.

Since the spray is injected by an ultrasonic nebulizer, the droplet size distribution produced is known to be approximately lognormal. Close to the jet wall the measured droplet size PDF shows a bias towards small droplets. According to Chrigui et al.

[7, 9, 40] the drop deformation regime map as a function of We and *Oh*, provided by Faeth [12], was used for determining if further droplet deformation or break up occurred in the spray jets. Here the Weber number was found to be less than 0.3 and Oh was less than 0.006 for droplets in the sizes range $40 < D_p < 50\ \mu$. Thus the droplets are assumed spherical and will not undergo any further deformation due to droplet break up, downstream of the nozzle exit plane. The simulations are performed using 12 different classes of droplets. It is remarkable that almost all classes possess the same injection axial velocity that eqnals 42 m/s, whereas the standard deviation corresponds to ca. 3 m/s yielding an axial turbulence intensity of 7.5 %.

3.3 Numerical Implementation

According to Chrigui et al. [7, 9, 40] the governing eqnations of the carrier gas phase are discretized in the 3D low-Mach number LES code FASTEST. The code is able to compute 3D-complex geometries by using flexible, block structured and boundary fitted grids [21, 29]. The code uses the finite volume method in which a co-located grid is applied. For spatial discretization, specialized central differencing schemes that hold the second order for arbitrary grid cells are used [21]. The convective term in the scalar transport is discretized using non-oscillatory, bounded TVD schemes. For the time stepping, multiple stage Runge-Kutta schemes with second order accuracy are used. A fractional step formulation is applied and at each stage a momentum correction is carried out in order to satisfy continuity. The parcels are tracked using LAG3D code in which the eqnation of motion, the temperature evolution and the evaporation rate are discretized using Euler first/second order schemes and solved explicitly [7–10, 39, 40].

4 Results and Discussions

Let us first compare the reference flames EtF3 and AcF3 using both the ethanol and the acetone fuel, in Fig. 2. Here the instantaneous contours of the OH mass fraction are plotted in the cross section along the center line for EtF3 and AcF3. The maximum value is obviously registered at the reaction zone where mixture fraction is close to stoichiometry. Downstream of the nozzle exit and at the centerline of the configuration, no flame is observed, probably caused by the high strain rate at the nozzle exit plane or by a lack of sufficient heat to maintain the combustion at the centerline. Further downstream, at $y = 0.3D$, due to momentum transfer from axial to radial direction, the OH reaches the maximum value. At the centerline and downstream the nozzle the temperature should reduce its value below the inlet boundary condition because of spray evaporation. This heat loss effect is not considered in the modeling yet. Depending on the evaporation rate the temperature plot is changing. If droplets evaporate within the pre-vaporization zone completely, the combustion regime will be likely to demonstrate a premixed nature. Note that the flammability

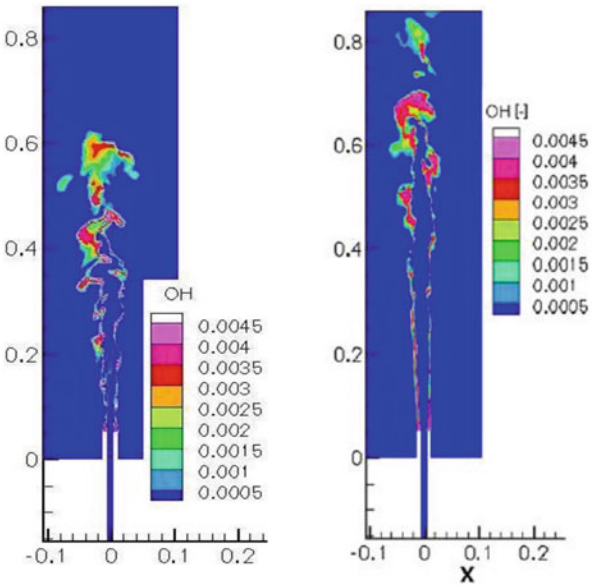

Fig. 2 Instantaneous plots of the OH mass fraction of the ethanol spray flame (*left*) and acetone flame (*right*) along the axial direction

limit of the ethanol lies between 0.44 and 3.34 while it is between 0.64 and 3.59 for the acetone. For very slow vaporization, i.e. most droplets exit the nozzle without evaporation; the spray flame is likely to have a diffusion flame behavior. Worth mentioning is that, numerically, the combustion cannot be sustained without setting the RPV boundary condition at the pilot flame location to its maximum value. An initialization of the RPV at the nozzle exit plane is not enough to make the mixture burn, because the RPV is transported downstream and the mixture blows out. In order to stabilize the flame, an initialization reqnires a recirculation zone which is not present in this configuration. The OH mass fraction, which is an indicator of the position of the flame, varies between "0" and 4.5×10^{-3} in both flames. However, the acetone flame appears higher than the ethanol one (see also Figs. 7 and 8).

Figures 3, 4, 5 and 6 show the axial droplet velocities and corresponding fluctuations of all the cases under investigation. Reasonable agreement for the mean droplet velocities is observed in the first cross-section. At x/D = 20 and x/D = 30, small discrepancies are observed in the averaged droplet velocity in the ethanol case. Unfortunately, a comparison between simulated gas phase velocity (that may help to clarify these discrepancies) and experimental data of the carrier phase (that are not available) is not possible. Disagreement at the last cross-sections may originate from the presence of remaining big droplets which are not following the carrier phase.

As the gas phase is captured using LES, mean velocities of droplets are well predicted. The axial velocity of the acetone test cases shows, at x/D = 30, an increase of its value compared to ethanol. Acetone is more volatile and has a lower boiling point than ethanol, thus it evaporates faster. The added vapor mass within a control volume accelerates the carrier phase, which drags the disperse phase faster, causing thus the

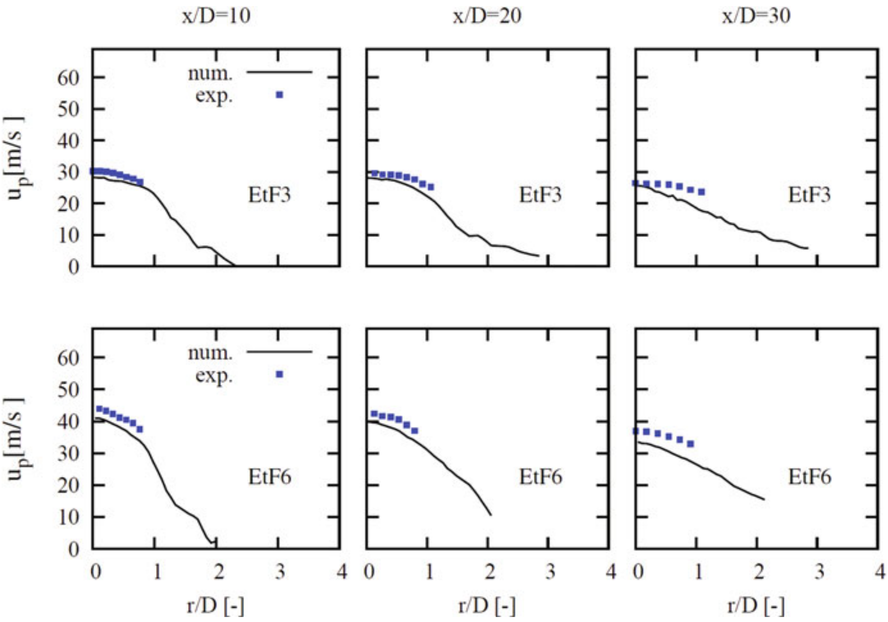

Fig. 3 Radial profiles of the droplet mean axial velocity at different distances from the nozzle exit plane for ethanol case. The x-axis represents r/D

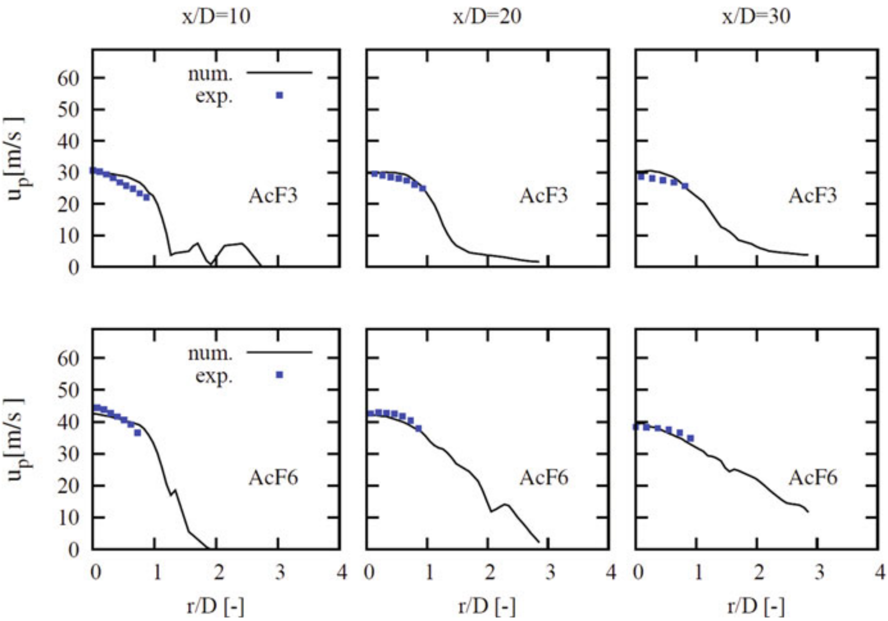

Fig. 4 Radial profiles of the droplet mean axial velocity at different distances from the nozzle exit plane for acetone case. The x-axis represents r/D

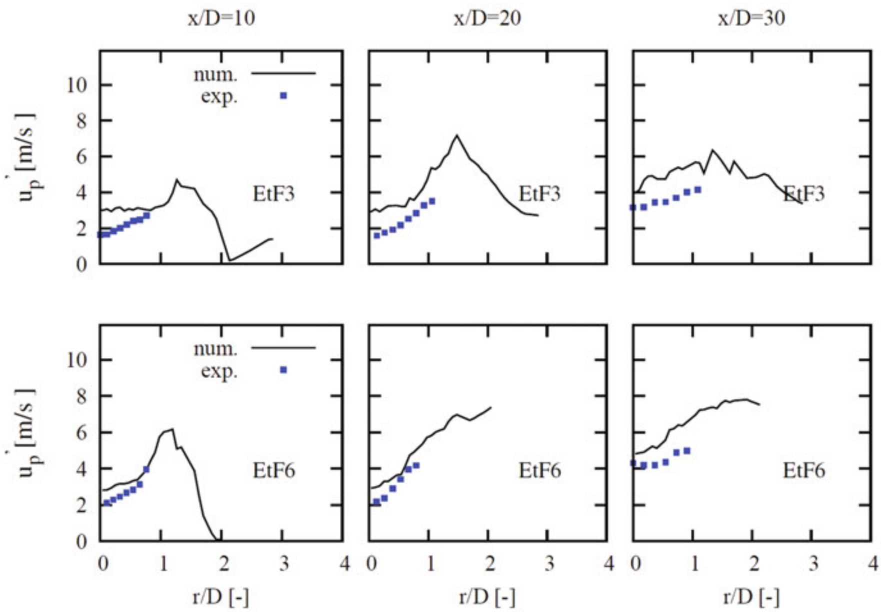

Fig. 5 Radial profiles of the droplet axial velocity fluctuation at different distances from the nozzle exit plane for ethanol. The x-axis represents r/D

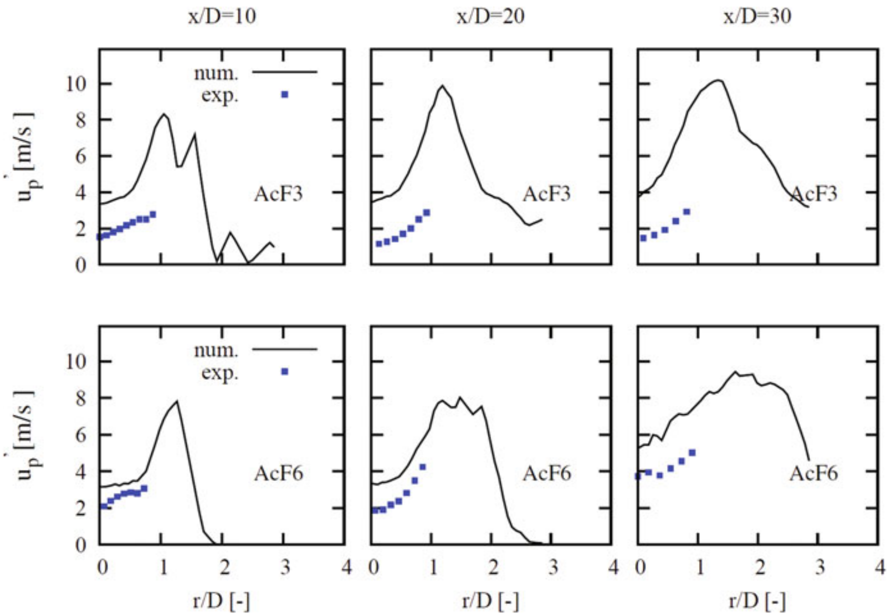

Fig. 6 Radial profiles of the droplet axial velocity fluctuation at different distances from the nozzle exit plane for acetone. The x-axis represents r/D

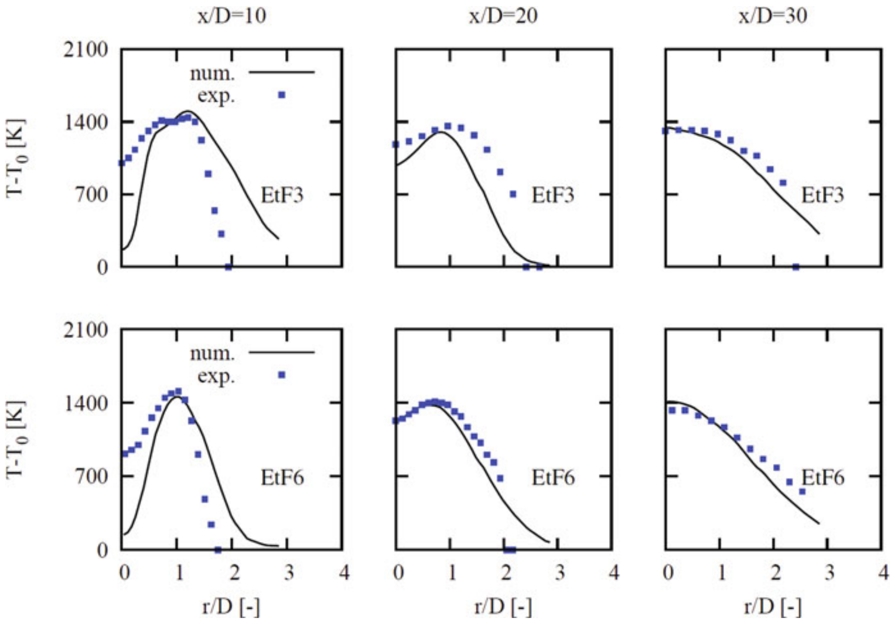

Fig. 7 Radial profiles of the excess temperature at different distances from the nozzle exit plane for ethanol. The x-axis represents r/D

increase of the droplet mean velocities. Worth noting is that the measurements are restricted to r/D = 1 since the number of droplets outside this region is not important and delivers no accurate statistics. The fluctuations of the droplet velocities of both fuels are comparable. The effect of faster evaporation is not remarkable. Numerically, acetone droplets show a higher RMS, particularly at the shear flow region, i.e. between the central jet and the co-flow. The difference between both fuels in the droplet velocity fluctuation is most likely caused by the difference in the droplet diameters. As acetone evaporates faster, corresponding droplets are more sensitive to the turbulence. Acetone droplets rather tend to follow the carrier phase dynamics than ethanol droplets, thus their RMS gets increased because of the important velocity gradient between r/D = 1 and r/D = 2.

The discrepancies between the experimental and numerical results in the droplet velocity fluctuations, observed in Figs. 5 and 6, could be caused by the spray-wall interaction, which is not modeled. At the nozzle exit, droplets are observed accumulating in the region close to the nozzle edge. A dense region is formed, thus collision and/or coalescence as well as breakup phenomena are likely to take place. As result, droplets are highly disturbed; they change their velocity and direction. Hence the turbulence level of the dispersed phase increases. The neglect of the effect of SGS on the dispersion of the spray may be another source of the discrepancies in the droplet fluctuations. Indeed small particles, as it is the general case in evaporating droplets, tend to follow the carrier phase dynamics, which is captured by the resolved part and the SGS contribution. This SGS dispersion is unfortunately not included yet.

The temperature plot in Figs. 7 and 8 is a function of the RPV, mixture fraction and corresponding variances. Using these variables as input parameters to the FGM

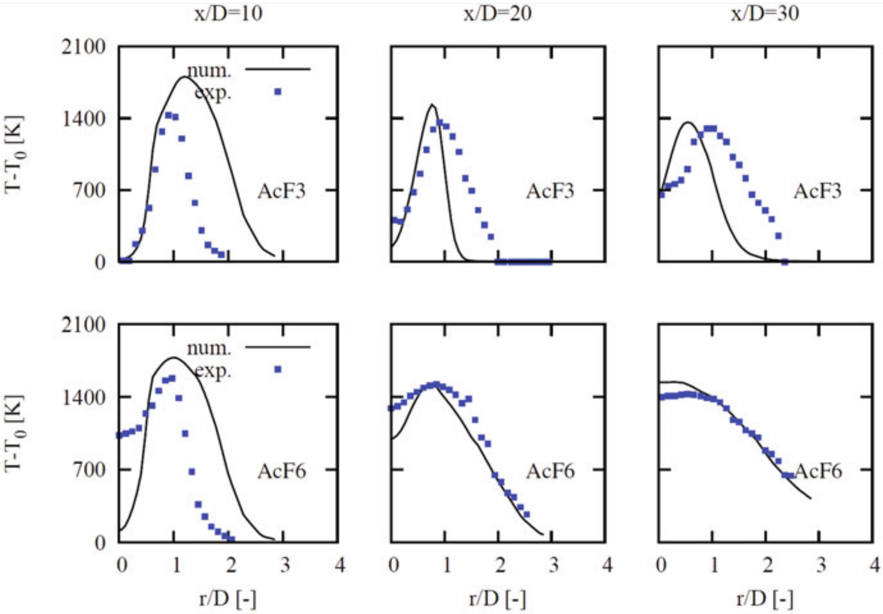

Fig. 8 Radial profiles of the excess temperature at different distances from the nozzle exit plane for ethanol. The x-axis represents r/D

table, the temperature is determined at each cell of the computational domain. It varies between the temperature of pure mixing and the maximum in case of eqnilibrium combustion. It is possible for the highest value of the RPV that different temperatures could be observed, depending on the mixture fraction and its variance. The center line of the configuration shows a cold flow despite the fact that the mixture fraction is close to stoichiometry.

Ethanol flames are broader and demonstrate an important value at the center line, i.e. $r/D = 0$. The mixture fraction distribution is altered by the rate of vaporization. The difference on the temperature profiles may also originate from the reaction mechanism, which involves different species and reactions number as well as laminar burning velocities. The numerical simulations show that the prediction of the ethanol flame agrees most favorably with the experimental data.

Figures 9 and 10 show the droplet volume flux at different axial cross- sections for ethanol and acetone, respectively. The numerical simulations predict the volume flux well and show reasonable agreements with the measurements. The slight over-prediction is expected, since not all droplets that cross a section could be experimentally captured, validated and registered. The real and correct profile of the droplet volume flux should be higher than the experimental curves provide. A comparison between the plots in Figs. 9 and 10 shows that the volume fluxes of acetone is smaller than that of ethanol. This indicates that the evaporation of the ethanol is slower than that of acetone.

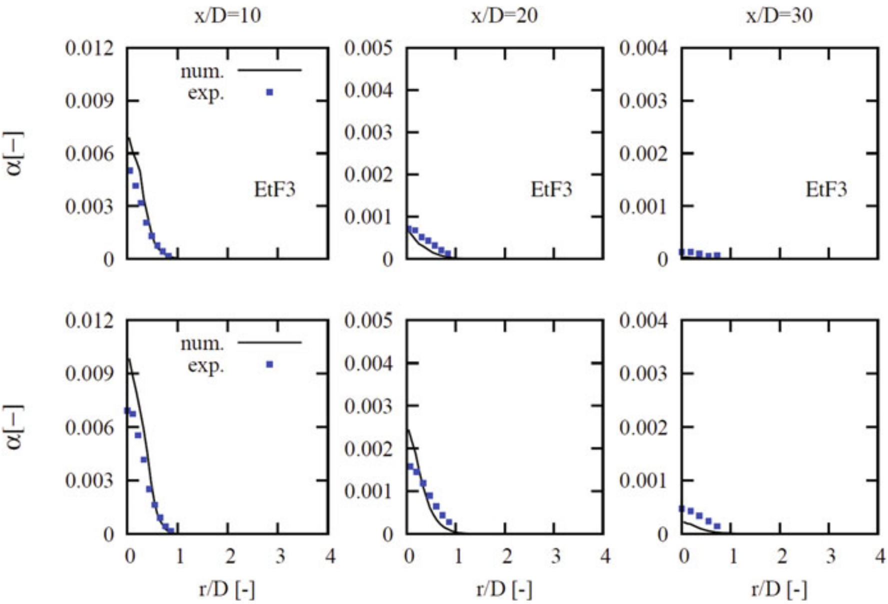

Fig. 9 Radial profiles of the droplet volume flux at different distances from the nozzle exit plane for ethanol. The x-axis represents r/D

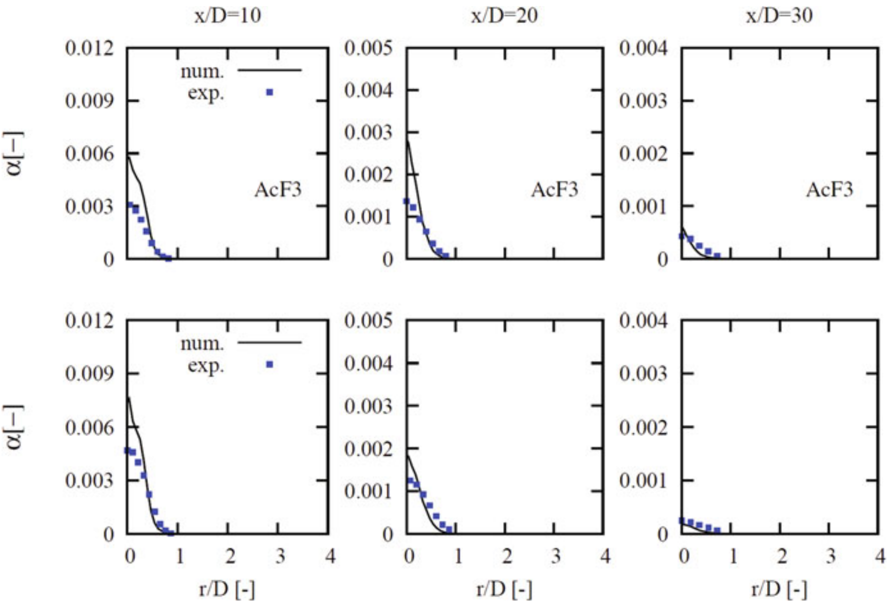

Fig. 10 Radial profiles of the droplet volume flux at different distances from the nozzle exit plane for acetone. The x-axis represents r/D

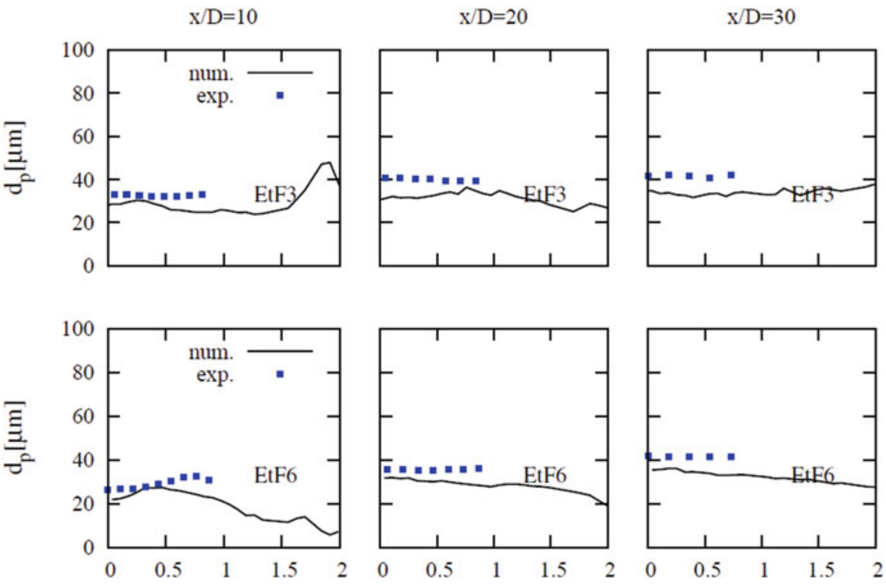

Fig. 11 Radial profiles of the droplet mean diameter at different distances from the nozzle exit plane for ethanol. The x-axis represents r/D

Figures 11 and 12 display the droplet mean-diameters for the ethanol and acetone spray at different cross-sections, respectively. A good agreement between the experimental data and the numerical simulation for all test cases is observed. Both sprays show similar behavior and evaporate in a comparable way. The acetone flame shows at x/D = 20 a lower diameter profile compared to ethanol which confirm that the acetone evaporates slightly faster.

Though the dispersed phase includes 12 different classes and demonstrates a polydisperse flow, the spray mean-diameters show nearly constant uniform profiles. This effect may be caused by the quick vaporization of the small classes that includes small droplet diameters, i.e. below 20 μm. Larger droplets, however, evaporate slower, they are dragged from the injection location to the nozzle exit within a highly turbulent flow, which increases the homogeneity of the class distribution in the prevaporization zone. Thus the spray mean diameter shows an approximately uniform profile in the radial direction.

5 Conclusion

An LES based investigation was carried out to analyze and evaluate the impact of fuel and mass loading on turbulent spray combustion. To retrieve the flow, mixing and combustion properties, an Eulerian-Lagrangian approach was adopted. The method included a full two-way coupling between the interacting two phases in presence, while the evaporation process was described by a non-eqnilibrium vaporization model. The carrier phase turbulence was captured by a combustion LES technique.

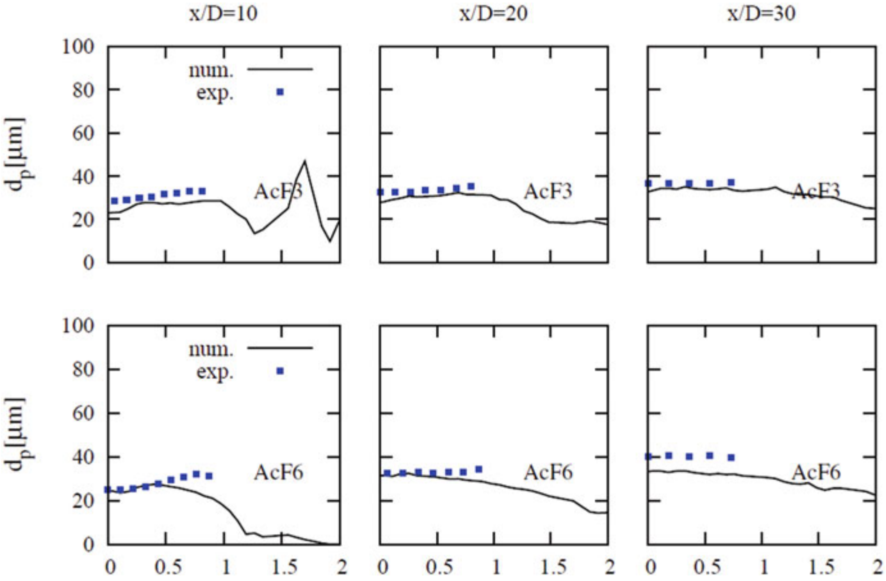

Fig. 12 Radial profiles of the droplet mean diameter at different distances from the nozzle exit plane for acetone. The x-axis represents r/D

In both cases, the ethanol and acetone fueled configurations, the occurring flow and combustion properties were numerically analyzed and compared with experimental data under different mass loading conditions. The impact of fuel and mass loading on turbulent spray combustion was evaluated in terms of flame structure, exhaust gas temperature, droplet diameters and velocities, droplet velocity fluctuations, and spray volume flux at different distances from the exit planes. The following conclusions can be drawn:

1. The axial droplet velocities predicted by simulations agree well with the experimental data. The discrepancies of the corresponding fluctuations can be attributed to the spray-wall interaction at the nozzle exit or/and to the deficiency of capturing the resolved instantaneous fluid velocity. This shows the necessity of a SGS dispersion model for evaporating droplets.
2. Acetone, which has a lower boiling point than ethanol, evaporates faster. This effect increases the carrier phase velocity, which in turn increases the drag of the spray, making thus the droplets move faster. The rate of vaporization influences the formation of the fuel/air mixture. The resulting mixture fraction of acetone/air demonstrates a richer character at the pre-vaporization zone and tends to a premixed behavior rather than the ethanol test cases.
3. The spray volume flow rates are in acceptable agreement. Thereby the simulation reveals the importance of polydispersity and accounts better for the actual amount of droplets than the experimental measurements.
4. With respect to spray combustion properties, the FGM concept captured well the flame height and lift-off. Although the effect of droplets on the thermocouple is

not quantified, spray evaporation and/or single droplet combustion at the thermocouple surface can produce large errors (up to 20 %). The temperature profiles demonstrated a fair agreement with the measurements.

In order to improve the results of the temperature, heat losses due to radiation and heat sinks because of spray evaporation should be considered.

Further improvements are suitable. The group combustion, that influences the spray combustion, should not be disregarded in the modeling. Droplet-droplet interaction along with the spray wall interaction should be added to improve the prediction of droplet distribution at the exit plane. An accurate SGS dispersion model needs to be integrated. It is also of great interest to generate the FGM table under consideration of the droplet vaporization process.

Acknowledgements The financial support by the Deutsche Forschungsgemeinschaft (DFG) is highly recognized.

References

1. B. Abramzon and W. A. Sirignano, Droplet Vaporization Model for Spray Combustion Calculations, Int. J. Heat Mass Transfer, Vol. 32, 1989, pp. 1605–1618.
2. S. V. Apte, K.Mahesh, M. Gorokhovski, P. Moin, Stochastic modeling of atomizing spray in a complex swirl injector using large eddy simulation, Proceedings of the Combustion Institute, Volume 32, Issue 2, 2009, Pages 2257–2266.
3. J. Bellan, L.C. Selle, Large Eddy Simulation composition eqnations for single-phase and two-phase fully multicomponent flows Original, Proceedings of the Combustion Institute, Volume 32, Issue 2, 2009, Pages 2239–2246.
4. A. Berlemont M. S. Grancher and G. Gouesbet, Heat and mass transfer coupling between vaporizing droplets and turbulence using a Lagrangian approach, J. of. Heat and Mass Transfer Vol.38, 1995, 3023–3034.
5. R. W., Bilger, S. H., St°arner, and R. J., Kee, On reduced mechanisms for methane-air combustion in nonpremixed flames. Combustion and Flame, 80, 1990, pp 135–149.
6. CHEM1D. http://www.tue.nl/en/university/departments/mechanical-engineering/research/research-groups/combustion-technology/flamecodes/chem1d/.
7. M. Chrigui, J. Gounder, A. Sadiki, A. R. Masri, J. Janicka, Partially premixed reacting acetone spray using LES and FGM tabulated chemistry, Combustion and Flame, Volume 159, Issue 8, Pages 2718–2741, August 2012.
8. M. Chrigui, J. Gounder, A. Sadiki, A. R. Masri, J. Janicka, Acetone Droplet Behavior in Reacting and Non Reacting Turbulent Flow, Flow Turbulence and Combustion, Volume 90, Issue 2, pp 419–447, 2013.
9. M. Chrigui, A. R. Masri, Amsini Sadiki, Johannes Janicka, Large Eddy Simulation of a Polydisperse Ethanol Spray Flame, Flow Turbulence and Combustion, Volume 90, Issue 4, pp 813–832, June 2013.
10. M. Chrigui, F. Sacomano, A. Sadiki A. R. Masri, Evaporation Modeling for Polydisperse Spray in Turbulent Flow, (present book), TCS3-Book-chapter.
11. U. Eguz, L.M.T. Somers, L.P.H. de Goey, Modeling of PCCI Combustion with the FGM approach, 13th International Conference on Numerical Combustion April 27–29, 2011, Corfu, Greece.
12. G. M. Faeth, Spray combustion phenomena, Proc. Combust. Inst. 26,1996, pp 1593–1612.

13. B. Fiorina, O. Gicquel, L. Vervisch, S. carpentier, N. Darabiha: Premixed turbulent combustion modeling using tabulated detailed chemistry and PDF, Proc. of the combustion institute, Vol. 30, pp. 867–874 (2005).
14. H.W. Ge and E. Gutheil, Probability density function (pdf) simulation of turbulent spray flows, Atomiz. Sprays 16 (2006), pp. 531–542.
15. M. Germano, U. Piomelli, P. Moin, and W. H. Cabot, A dynamic sub-grid scale eddy viscosity model, 1991, Phys. Fluids A, 3: 1760–1765.
16. J. D. Gounder and A. R. Masri, Flow field and Mass Flux Measurements near the Exit Plane of Spray Jets, ICLASS 2009, 11th Triennial International Annual Conference on Liquid Atomization and Spray Systems, Vail, Colorado USA, July 2009.
17. E. Gutheil, Modeling and Simulation of Droplet and Spray Combustion, Handbook of combustion, Wiley-VCH Verlag GmbH & Co. KGaA, 2010.
18. J. Janicka, A. Sadiki: Large Eddy Simulation of turbulent combustion systems, Proc. Of the combustion institute, 30, pp. 537–547, 2005.
19. W.P. Jones, S. Lyra, A.J. Marquis, Large Eddy Simulation of evaporating kerosene and acetone sprays, International Journal of Heat and Mass Transfer, Vol. 53, Issues 11–12, 2010, Pages 2491–2505.
20. T. Landenfeld, A. Sadiki, J. Janicka, A Turbulence-Chemistry Interaction Model Based on a Multivariate Presumed Beta-PDF Method for Turbulent Flames, Flow, Turbulence and Combustion, Volume 68,Issue 2, 2002, pp 111–135.
21. T. Lehnhäuser and M. Schäfer. Improved linear interpolation practice for finitevolume schemes on complex grids. Int. J. Numer. Meth. Fluids, 38(7), 2002, pp 625–645.
22. N. M. Marinov: A detailed chemical kinetic model for high temperature ethanol oxidation. Int. J. Chem. Kinet., 31: 183–220, 1999.
23. A. R. Masri, J. D. Gounder, Turbulent Spray Flames of Acetone and Ethanol Approaching Extinction, Journal: Combustion Science and Technology, vol. 182, 2010, pp. 702–715.
24. A. Milford, C.B. Devaud, Investigation of an inhomogeneous turbulent mixing model for conditional moment closure applied to autoignition, Comb. and Flame, Vol. 157, Issue 8, 2010, Pages 1467–1483.
25. R. S. Miller, K. Harstad, and J. Bellan. Evaluation of eqnilibrium and non-eqnilibrium evaporation models for many gas-liquid flow simulations. Int. J. Multiphase Flow, 24:1026–1055, 1998.
26. M. Mortensen, R. W. Bilger "Derivation of the conditional moment closure eqnations for spray combustion" Combustion and Flame, Volume 156, Issue 1, 2009, Pages 62–72.
27. S. Navarro-Martinez, A. Kronenburg, LES–CMC simulations of a lifted methane flame, Proceedings of the Combustion Institute, Volume 32, Issue 1, 2009, Pages 1509–1516.
28. A. Neophytou, E. Mastorakos, R.S. Cant, Complex chemistry simulations of spark ignition in turbulent sprays, Proceedings of the Combustion Institute, Volume 33, Issue 2, 2011, Pages 2135–2142.
29. C. Olbricht, A. Ketelheun, F. Hahn and J. Janicka, Assessing the predictive capabilities of Combustion LES as applied to the Sydney flame series, Flow Turbulence and Combustion, 83 (3), 2011, pp 513–547.
30. N. Patel and S. Menon, Simulation of spray–turbulence–flame interactions in a lean direct injection combustor, Combustion and Flame, Volume 153, Issues 1–2, April 2008, Pages 228–257.
31. C. Pera, J. Réveillon, L. Vervisch, P. Domingo, Modeling subgrid scale mixture fraction variance in LES of evaporating spray, Combustion and Flame, Volume 146, Issue 4, September 2006, Pages 635–648.
32. Cécile Pera, Julien Réveillon, Luc Vervisch, Pascale Domingo, Modeling subgrid scale mixture fraction variance in LES of evaporating spray, Combustion and Flame, Volume 146, Issue 4, 2006, Pages 635–648.
33. N. Peters, Laminar diffusion flamelet models in non-premixed turbulent combustion, Progress in Energy and Combustion Science, vol. 10, Issue 3, 1984, pp 319–339.

34. S. Pichon, G. Black, N. Chaumeix, M. Yahyaoui, J.M. Simmie, H. J. Curran, R. Donohue, The combustion chemistry of a fuel tracer: Measured flame speeds and ignition delays and a detailed chemical kinetic model for the oxidation of acetone, Com. & Flame, Vol. 156, 2009, pp 494–504.
35. C. Pierce and P. Moin, Progress variable approach for large eddy simulation of turbulent non-premixed combustion, J. Fluid Mechanic, Vol. 504:73–97.
36. H.Pitsch: Large-Eddy Simulation of Turbulent Combustion, Annual Re-view of Fluid Mechanics, Vol. 38: 453–482, 2006.
37. T. Poinsot and D. Veynante, Theoretical and Numerical Combustion, 3rd Edition, (2011).
38. J. Pozorski, S.A. Apte: Filtered particle tracking in isotropic turbulence and stochastic modeling of subgrid-scale dispersion, Int. J.of Multiph. Flow, Vol. 35 (2) pp. 118–128, 2009.
39. A. Sadiki, W. Ahmadi, M. Chrigui, Toward the Impact of Fuel Evaporation-Combustion Interaction on Spray Combustion in Gas Turbine Combustion Chambers. Part I: Effect of Partial Fuel Vaporization on Spray Combustion. Chapter in Experiments and Numerical Simulations of Diluted Spray Turbulent Combustion, Proceedings of the 1st International Workshop on Turbulent Spray Combustion, Series: ERCOFTAC Series, Vol. 17, Merci, Bart; Roekaerts, Dirk; SADIKI, AMSINI (Eds.), 2011.
40. A. Sadiki, M. Chrigui, and A. Dreizler, Thermodynamically Consistent Modelling of Gas Turbine Combustion Sprays, Fluid Mechanics and Its Applications 102, Flow and Combustion in Advanced Gas Turbine Combustors DOI 10.1007/978-94-007-5320-4 3.
41. A. Sadiki, M. Chrigui, J. Janicka, M.R. Maneshkarimi, Modeling and Simulation of Effects of Turbulence on Vaporization, Mixing and Combustion of Liquid-Fuel Sprays, In: Flow Turb. Comb., 75 (1–4), (2005).
42. P. Sagaut, Large Eddy Simulation for incompressible Flows, Springer, Berlin, 2001.
43. M. Sanjosé, J.M. Senoner, F. Jaegle, B. Cuenot, S. Moreau, T. Poinsot, Fuel injection model for Euler–Euler and Euler–Lagrange large-eddy simulations of an evaporating spray inside an aeronautical combustor, International Journal of Multiphase Flow, Volume 37, Issue 5, June 2011, Pages 514–529.
44. S.S. Sazhin.: Advanced models for fuel droplet heating and evaporation, Progress in Energy and Combustion Science 32, pp. 162–214, 2006.
45. P. Schroll, A.P. Wandel, R.S. Cant, E. Mastorakos, Direct numerical simulations of autoignition in turbulent two-phase flows, Proceedings of the Combustion Institute, Volume 32, Issue 2, 2009, Pages 2275–2282.
46. W. A. Sirignano, Fluid dynamics of sprays, J. Fluids Engng. Vol. 115, 1993, pp. 345–378.
47. S. H. Stårner, J. Gounder, and A. R. Masri, Effects of turbulence and carrier fluid on simple, turbulent spray jet flames, Com. & Flame, Vol. 143, 2005, pp 420–432.
48. J.A. Van Oijen, L.P.H. De Goey, A numerical study of confined triple flames using a flamelet-generated manifold, Combust. Theory Modelling, 2004, pp 141–163.
49. O. Vermorel, S. Richard, O. Colin, C. Angelberger, A. Benkenida, D. Veynante, Towards the understanding of cyclic variability in a spark ignited engine using multi-cycle LES, Combustion and Flame, Volume 156, Issue 8, August 2009, Pages 1525–1541.
50. A. W. Vreman, B. A. Albrecht, J. A. van Oijen, L. P. H. de Goey, R. J. M. Bastiaans: Premixed and non-premixed generated manifolds in large-eddy simulation of Sandia flame D and F. Combust Flame 153, 394–416, 2008.
51. B. Wegner, A. Maltsev, C., Schneider, A., Sadiki, A., Dreizler, J., Janicka, Assessment of unsteady RANS in predicting swirl flow instability based on LES and Experiments. International Journal of Heat and Fluid Flow, 2004, 25:528–536.
52. M.R.G. Zoby, S. Navarro-Martinez, A. Kronenburg, A.J. Marquis, Evaporation rates of droplet arrays in turbulent reacting flows, Proceedings of the Combustion Institute, Volume 33, Issue 2, 2011, Pages 2117–2125.